ELSEVIER

Journal of Atmospheric and Solar-Terrestrial Physics 68 (2006) 629–638

Journal of ATMOSPHERIC AND SOLAR-TERRESTRIAL PHYSICS

www.elsevier.com/locate/jastp

InSAR tropospheric delay mitigation by GPS observations: A case study in Tokyo area

Caijun Xu[a,*], Hua Wang[a], Linlin Ge[b], Chinatsu Yonezawa[c], Pu Cheng[a]

[a]*School of Geodesy and Geomatics, The Key Laboratory of Geo-space Environment and Geodesy, Ministry of Education, Wuhan University, 129 Luoyu Road, Wuhan 430079, China*

[b]*School of Surveying & Spatial Information Systems, The University of New South Wales, Sydney NSW 2052, Australia*

[c]*Remote Sensing Technology Center of Japan, Roppongi First Bldg, 12F, 1-9-9, Roppongi, Minato-ku, Tokyo 1060032, Japan*

Received 26 January 2005; received in revised form 29 October 2005; accepted 5 November 2005
Available online 23 January 2006

Abstract

Like other space geodetic techniques, interferometric synthetic aperture radar (InSAR) is limited by the variations of tropospheric delay noise. In this paper, we analyze the double-difference (DD) feature of tropospheric delay noise in SAR interferogram. By processing the ERS-2 radar pair, we find some tropospheric delay fringes, which have similar patterns with the GMS-5 visible-channel images acquired at almost the same epoch. Thirty-five continuous GPS (CGPS) stations are distributed in the radar scene. We analyze the GPS data by GIPSY-OASIS (II) software and extract the wet zenith delay (WZD) parameters at each station at the same epoch with the master and the slave image, respectively. A cosine mapping function is applied to transform the WZD to wet slant delay (WSD) in line-of-sight direction. Based on the DD WSD parameters, we establish a two-dimensional (2D) semi-variogram model, with the parameters 35.2, 3.6 and 0.88. Then we predict the DD WSD parameters by the kriging algorithm for each pixel of the interferogram, and subtract it from the unwrapped phase. Comparisons between CGPS and InSAR range changes in LOS direction show that the root of mean squares (RMS) decreased from 1.33 cm before correction to 0.87 cm after correction. From the result, we can conclude that GPS WZD parameters can be effectively used to identify and mitigate the large-scale InSAR tropospheric delay noise if the spatial resolution of GPS stations is dense enough.

Keywords: InSAR; Wet zenith delay; Wet slant delay; Double difference; Semi-variogram model; Kriging

1. Introduction

In the past 2 decades, interferometric synthetic aperture radar (InSAR) has been widely used in the measurement of topography, surface deformation and flow velocities (cf. Massonnet and Feigl, 1998; Rosen et al., 2000; Hanssen, 2001). In all of the above applications, the useful information is obtained from the interferogram by the complex conjugation of the master image and the slave image. Like any other space geodetic technique, InSAR is also limited by the spatial and temporal variations of atmospheric delay noise. The early reports on the atmospheric delay effect in the interferogram can be referred to Massonnet et al.

*Corresponding author. Tel.: +86 27 68778805; fax: +86 27 68778371.
E-mail addresses: cjxu@sgg.whu.edu.cn, cjxu2008@hotmail.com (C. Xu).

1364-6826/$ - see front matter © 2006 Elsevier Ltd. All rights reserved.
doi:10.1016/j.jastp.2005.11.010

(1994), Tarayre and Massonnet (1996), Massonnet and Feigl (1995), Bevis et al. (1996), Rigo and Massonnet (1999), and Goldstein (1995).

Since the similar aspect in the interferogram is caused by geophysical signal and atmospheric artifact, it is difficult to discriminate them directly (Massonnet and Feigl, 1995). Studies on InSAR atmospheric errors have been carried out both in stochastic and deterministic ways. Through spatial spectrum analysis of delay features in the interferogram observed in Mojave desert in California, Goldstein (1995) found the $-8/3$ power-law for the spectrum of the atmospheric delay noise, and deduced that the noise was mostly caused by water vapor turbulence. In more detail, Hanssen (1998) analyzed a set of 26 tandem ERS SAR differential interferograms, covering relatively flat areas around the Dutch provinces Groningen and Flevoland, and found that the power spectra of the atmospheric delay noise in all of the interferograms were consistent with the Kolmogorov turbulence theory. The methods on the mitigation of InSAR atmospheric delay noise can be classified into two categories: statistical method (e.g. Zebker et al., 1997; Emardson et al., 2003) and calibration method (e.g. Delacourt et al., 1998; Williams et al., 1998). In the statistical method, the atmospheric delay noise is regarded as white noise, and multiple independent interferograms of the same area are stacked to reduce the artifact. Although this method is easy to carry out, it has at least two limitations: the deformation is assumed to be stable during different interferograms, which is not often the truth for geophysical process, besides, many independent pairs with high coherence are needed for stacking. In the calibration method, the atmospheric delay parameters from independent sources, such as meteorology, GPS, etc., are used. In spite of the lower spatial resolution of these sources, it is still feasible because of the power-law nature of the atmospheric delay noise variation (Williams et al., 1998). Delacourt et al. (1998) applied a semi-empirical approach with ground-based meteorological parameters to calibrate the interferogram in Etna. The tropospheric delay with the accuracy of 1 cm can be obtained by continuous GPS (CGPS) network observations (Williams et al., 1998). Thus GPS or the integration of GPS and meteorology data will be an optimal method to mitigate the atmospheric delay in InSAR. Several studies on the mitigation of InSAR atmospheric delay noise by GPS wet zenith delay (WZD) have been carried out in SCIGN and Mount Etna area (e.g. Bonforte et al., 2001; Wadge et al., 2002; Li et al., 2003, 2004, 2005; Buckley et al., 2003). As one of the densest CGPS arrays in the world, GEONET can also play an important role in InSAR atmospheric delay study. Tokyo, which is surrounded by Tokyo Bay, tends to be affected by atmospheric delay. Yonezawa and Takeuchi (2003) found the atmospheric delay fringe patterns in the interferograms in Tokyo area. With CGPS WZD data in the same area, Janssen et al. (2004) analyzed different interpolation algorithms during the atmospheric delay mitigation. In this paper, we will first analyze the atmospheric delay effect in SAR interferogram. Then, using the same SAR images and CGPS measurements with those used by Yonezawa and Takeuchi (2003) and Janssen et al. (2004), we will utilize the double-difference (DD) model and geostatistical algorithm to mitigate the atmospheric delay noise in the interferogram.

2. Atmospheric delay feature in repeat-pass InSAR

The atmospheric delay consists of bending and propagation delay (Bean and Dutton, 1968). Bean and Dutton (1968) have shown that even for extreme refractivity, the bending error can be neglected for zenith angles less than 87°. Therefore, only propagation delay will affect InSAR for the small zenith angle of these satellites. Thus, the total zenith atmospheric delay can be expressed as

$$\Delta r_{\mathrm{a}} = \Delta r_{\mathrm{h}} + \Delta r_{\mathrm{w}} + \Delta r_{\mathrm{l}} + \Delta r_{\mathrm{i}}, \tag{1}$$

where Δr_{h} is the hydrostatic zenith delay component, Δr_{w} is the WZD component caused by precipitable water vapor, Δr_{l} is the liquid zenith delay component caused by liquid water in the air and Δr_{i} is the ionospheric zenith delay component.

Considering the atmospheric delay error, the absolute phase for a point p in the coregistered master and slave image can be expressed as

$$\begin{aligned} \varphi_1 &= -\frac{4\pi}{\lambda}\left(r_1 + \Delta r^1_{\mathrm{a;p}}\right) + \varphi^1_{scat}, \\ \varphi_2 &= -\frac{4\pi}{\lambda}\left(r_2 + \Delta r^2_{\mathrm{a;p}}\right) + \varphi^2_{scat}, \end{aligned} \tag{2}$$

where λ is the wave length, φ^1_{scat} and φ^2_{scat} are the scattering phases, r_1, r_2 are the slant ranges, $\Delta r^1_{\mathrm{a;p}}$ and $\Delta r^2_{\mathrm{a;p}}$ are slant atmospheric delay in the master image and the slave image, respectively.

For repeat-pass InSAR, the interferometric phase is the phase difference between the master image

and the slave image if the scattering phase is regarded as invariant, see (3):

$$\varphi = \frac{4\pi}{\lambda}\left(r_1 - r_2 + \Delta r^1_{\mathrm{a;p}} - \Delta r^2_{\mathrm{a;p}}\right). \quad (3)$$

Therefore, the additional phase shift caused by the atmospheric delay can be expressed as

$$\Delta\varphi_{\mathrm{a}} = \frac{4\pi}{\lambda}\left(\Delta r^1_{\mathrm{a;p}} - \Delta r^2_{\mathrm{a;p}}\right) = \frac{4\pi}{\lambda}\Delta r^{1,2}_{\mathrm{a;p}}. \quad (4)$$

InSAR is a relative measurement, and only wrapped phase is recorded in the interferogram. After phase unwrapping, the unwrapped phase, instead of the absolute phase, can be obtained. Therefore, the information deduced from interferogram is relative to the reference point selected during phase unwrapping. From this point of view, the atmospheric delay after phase unwrapping can be accurately expressed as a *DD model*:

$$\Delta\varphi_{\mathrm{a}} = \frac{4\pi}{\lambda}\left(\Delta r^{1,2}_{\mathrm{a;p}} - \Delta r^{1,2}_{\mathrm{a};f}\right) = \frac{4\pi}{\lambda}\Delta r^{1,2}_{\mathrm{a;p},f}, \quad (5)$$

where the lower index f is the reference point during phase unwrapping. Since the temporal stability of the hydrostatic delay and the large-scale (>50 km) variation property of ionospheric delay in most cases (except for polar and equatorial area), both of them can be neglected in the interferogram for the DD model. Therefore, the total atmospheric delay for repeat-pass InSAR can be written as

$$\Delta\varphi_{\mathrm{a}} = \frac{4\pi}{\lambda}\Delta r^{1,2}_{\mathrm{a;p},f} = \frac{4\pi}{\lambda}\frac{1}{M(\theta)}\left(\Delta r^{1,2}_{\mathrm{w;p},f;} + \Delta r^{1,2}_{\mathrm{l;p},f}\right), \quad (6)$$

where $M(\theta)$ is the mapping function and θ is the zenith angle of ray in the air, $\Delta r^{1,2}_{\mathrm{w;p},f}$ is the DD WZD mainly caused by water vapor in the air, and $\Delta r^{1,2}_{\mathrm{l;p},f}$ is the DD liquid zenith delay caused by propagation through volume filled with liquid droplets. For a cumulus congestus, $\Delta r^{1,2}_{\mathrm{l;p},f}$ can be up to 5.6 mm, but it is less than 1 mm under usual atmospheric circumstances (Hanssen, 2001). Hence, for the atmospheric delays observed in the interferogram water vapor will be the main driving force. In many space geodetic techniques, e.g. GPS, the total wet delay is measured.

3. InSAR data and GPS measurement in Tokyo

In GEONET, 35 CGPS stations are distributed near the radar scene (24 stations are in the inner, and 11 ones are around) (Fig. 1). The average baseline length of the stations is about 15 km. We process the GPS observations with NASA/JPL

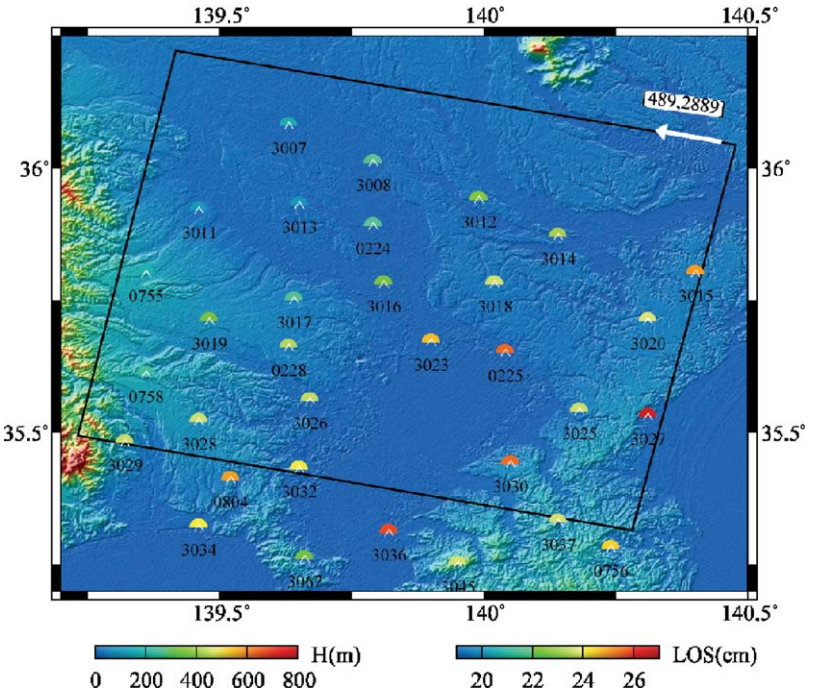

Fig. 1. DEM image and CGPS stations in Tokyo area. The background color represents the height of DEM. Each half-circle represents the position of CGPS station, and the inner color represents the LOS WZD. The black rectangular is the frame of radar images.

GIPSY-OASIS (II) software (Webb and Zumberge, 1993). Using the precise point positioning (PPP) method, we extract the WZD parameter, including Δr_w and Δr_l in Eq. (1), series for 5-min interval. By the average of the parameters 2-before and 2-after the radar epoch, we obtain the WZD parameter at each station for the interferogram. Using the cosine mapping function, i.e. $M(\theta) = \cos(23^\circ)$ in (6), the line-of-sight wet delay (WSD) can be obtained (Fig. 1). The peak-to-peak WSD difference is 85.8 mm between S3039 and S3013.

Two SAR images were acquired during descending passes of ERS-2 satellite at UTC 01:22 on February 8 and August 2, 1999 in Tokyo, Japan (Track 489/Frame 2889/Orbit 19882 and 22387). The SAR images were processed with Atlantis EV-InSAR software by the DEM-elimination (DEME) approach (Massonnet and Feigl, 1995). In this approach, the effect of topography was removed by an external DEM with the resolution of 50 m from the Geographical Survey Institute of Japan (Fig. 1). After interactive removal of the linear trend of orbit error, we obtained the interferogram (Fig. 2). The interferogram was unwrapped with SNAPHU software developed by Curtis W. Chen in Stanford University (Chen, 2001) (Fig. 3). The regions whose coherence is less than 0.2 are masked during phase unwrapping because SNAPHU will unwrap every pixel of the interferogram, even for those with zero coherence.

The Japanese Geostationary Meteorological Satellite (GMS-5) images are taken over the Tropical Western Pacific (TWP) region and over each of the TWP sites. It carries a Visible and Infrared Spin Scan Radiometer (VISSR) with four channels, one in the visible part of the spectrum and three in the infrared. The ground resolution is 1.25 km in the visible channel and 5 km in the infrared. We calculate the albedo difference with the GMS-5 visible-channel images obtained at 01:30 UTC on February 8 and August 2, 1999 (Fig. 4). It shows similar cloud patterns in Figs. 3 and 4, although there is about 8-min interval between them.

4. Semi-variogram model and universal kriging algorithm

The structure function is commonly used to investigate the spatial and temporal relationship between geospatial data separated by a vector h or span t (Goovaerts, 1997). Unlike the covariance and correlation function, which are measures of

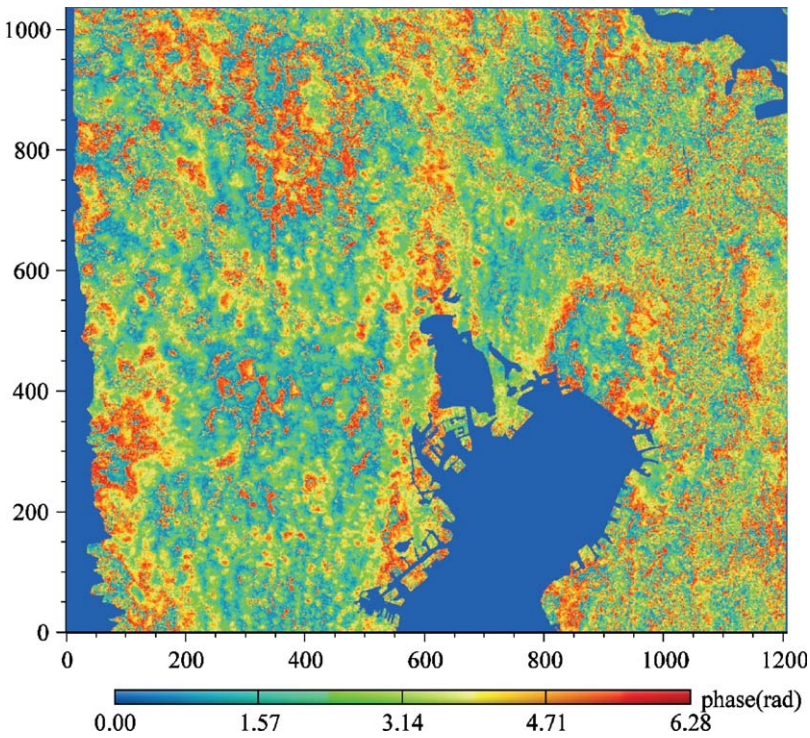

Fig. 2. Interferogram obtained by 990208/990802.

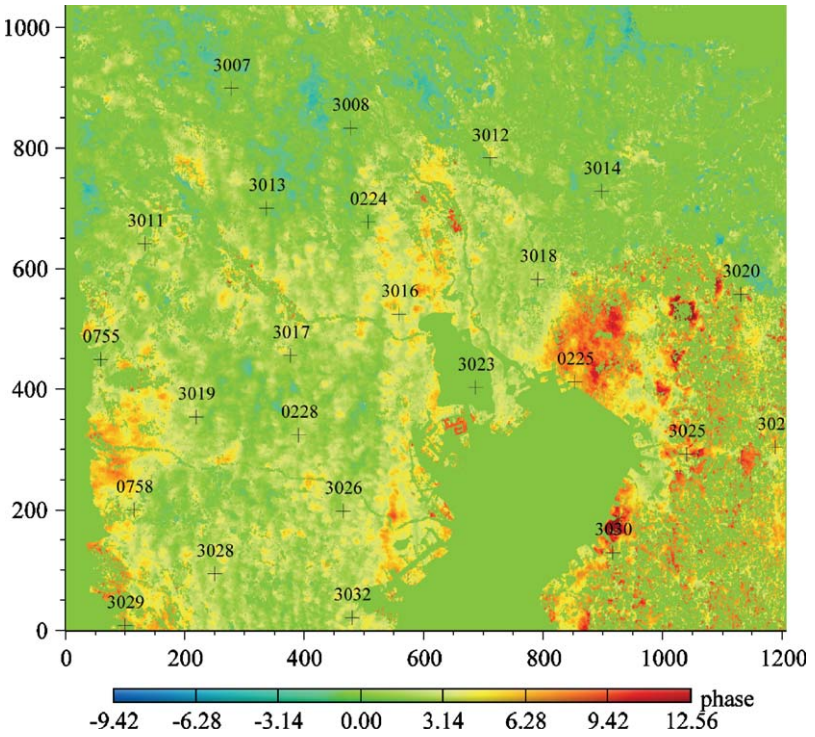

Fig. 3. Unwrapped phase with SNAPHU software.

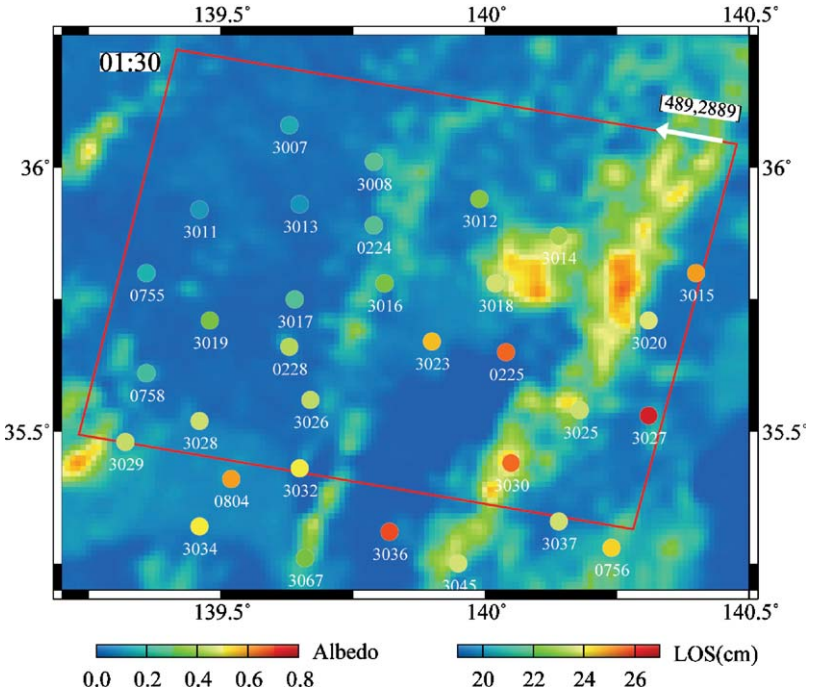

Fig. 4. Difference of the albedo images for Tokyo acquired by GMS-5 at 01:30 on February 8 and August 2, 1999.

similarity, the semi-variogram and variogram functions are the measures of dissimilarity between data. The semi-variogram function has already been used to investigate the variability of water vapor delay in GPS, InSAR and other space geodetic techniques (Goldstein, 1995; Hanssen, 1998; Emardson et al., 2003; Williams et al., 1998). All above studies have shown that the variation of water vapor conforms to the *Treuhaft and Lanyi* (TL) model on the assumptions of Kolmogorov turbulence theory (Treuhaft and Lanyi, 1987). Since the experimental variogram is a statistical value of the observations, the nugget effect, relating to measurement error and/or spatial sources of variation at distances smaller than the shortest sampling interval, must be considered. In the present study, we fit the semi-variogram model by a power model with the nugget effect using the robust estimation method (Cressie and Hawkins, 1980). Before calculation of the experimental semi-variogram, the linear trend has been removed. The final model in our study is

$$\hat{\gamma} = 35.2 + 3.6 \times h^{0.88}. \quad (7)$$

In TL model, the power index ranges from 2/3 for h up to O(10^3) km, and 5/3 for h smaller than 1 km. Hanssen (1998, 2001) also estimated the index close to 1 from the differential tandem InSAR pairs. Emardson et al. (2003) estimated that the value is close to 1 too. The power index in our estimation is 0.88, which is close to their studies. However, the nugget effect is neglected in the former two studies. Emardson et al. (2003) regarded the additional variance is caused by the height difference. In Tokyo area, the peak-to-peak height difference is less than 800 m, so we do not attribute the nugget effect to the height difference. In our model, the nugget effect is 35.2 mm^2, which should be caused by the WZD observation variance, ranging 25–81 mm^2 (Figs. 5 and 6).

Numerous of studies have confirmed that the kriging algorithm is most successful in the geospatial data prediction (Goovaerts, 1997). Firstly, kriging allows a great flexibility to control the characteristics of the prediction surface by the modification of variogram model. Secondly, it weighs the information locally, and the influence of a support point on the target value is controlled by the spatial correlation. In addition, kriging has the advantage to provide the expected mean square error of prediction in comparison with non-stochastic methods (Stein et al., 2002). In this study, the universal kriging (UK) algorithm is made use of to predict the wet delay. In UK, it is customary to

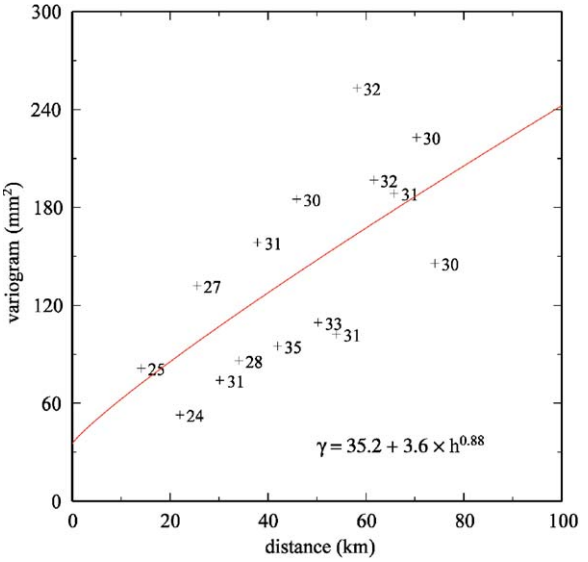

Fig. 5. Variogram model fitted by GPS LOS wet delay.

decompose the predicted value into a deterministic component, the so-called trend, which models the large-scale variation, and a stochastic component, modeling the smooth small-scale fluctuations and the irregular part of the variation. The general model of UK is given as follows:

$$\hat{Y}(s_0) = x_0'\hat{\beta} + \sigma'\Sigma^{-1}(Y - X\hat{\beta}), \quad (8)$$

where x_0 is the coordinates of prediction target, $\hat{\beta}$ is trend parameters estimated by the observations, X is the design matrix with the explanatory variables, Y denotes the vector with the random variables modelling the observations, and σ denotes an n-vector with the covariance between the values at the prediction and the observation locations, Σ is the matrix with the covariance of those random variables. $x_0'\hat{\beta}$ is deterministic component, and $\sigma'\Sigma^{-1}(Y - X\hat{\beta})$ is a stochastic component.

Four steps are accomplished in the prediction:

(1) Fitting the trend parameters $\hat{\beta}$ by a bi-linear function with the WSD parameters at the 35 stations.
(2) Calculating the experimental variogram and fitting the semi-variogram model.
(3) Calculating the weight $\sigma'\Sigma^{-1}$ by the semi-variogram model and the distance between support points and target points.
(4) Predicting the WSD at each pixel. Noting that the linear trend has been removed during orbit error correction, only the stochastic component will attribute to the artifact in the interferogram,

instead of adding the trend back. The peak-to-peak stochastic component is 40 mm in the predicted image (Fig. 7).

After UK prediction, we obtain the cleaned unwrapped phase by subtracting the WSD from the original unwrapped phase (Fig. 8). S0224 is

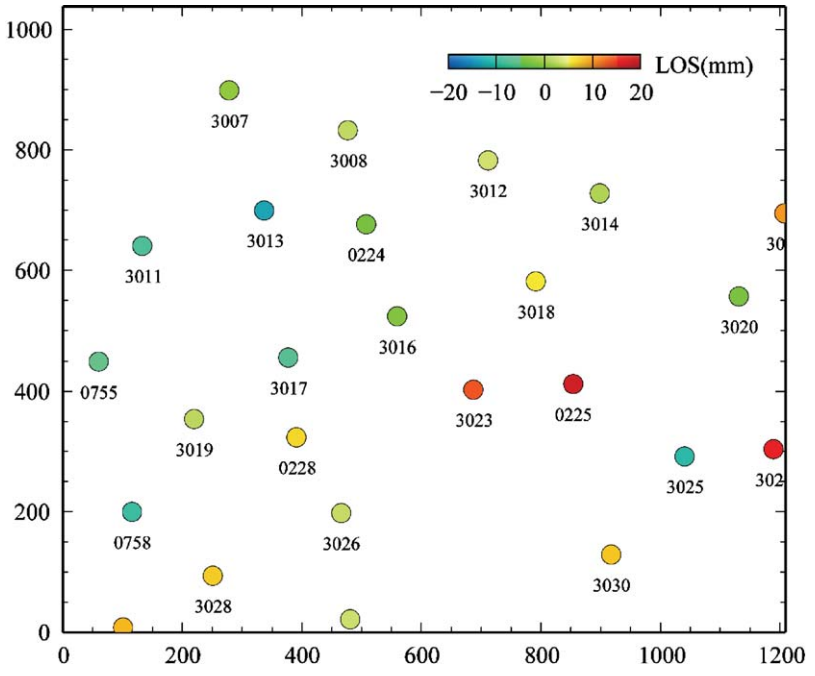

Fig. 6. The LOS wet delay after double difference and linear trend removal.

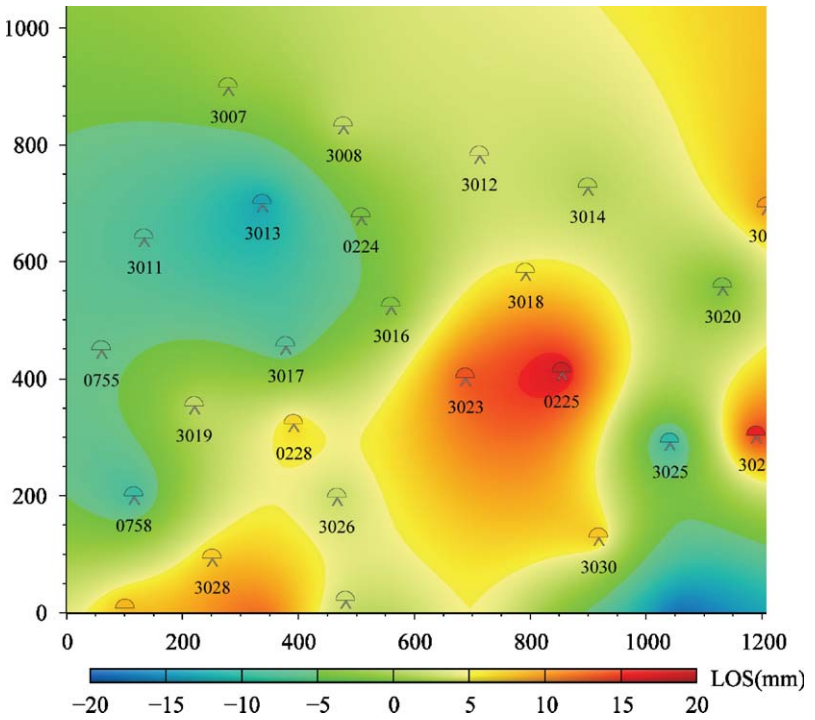

Fig. 7. Interpolated GPS LOS wet delay by UK.

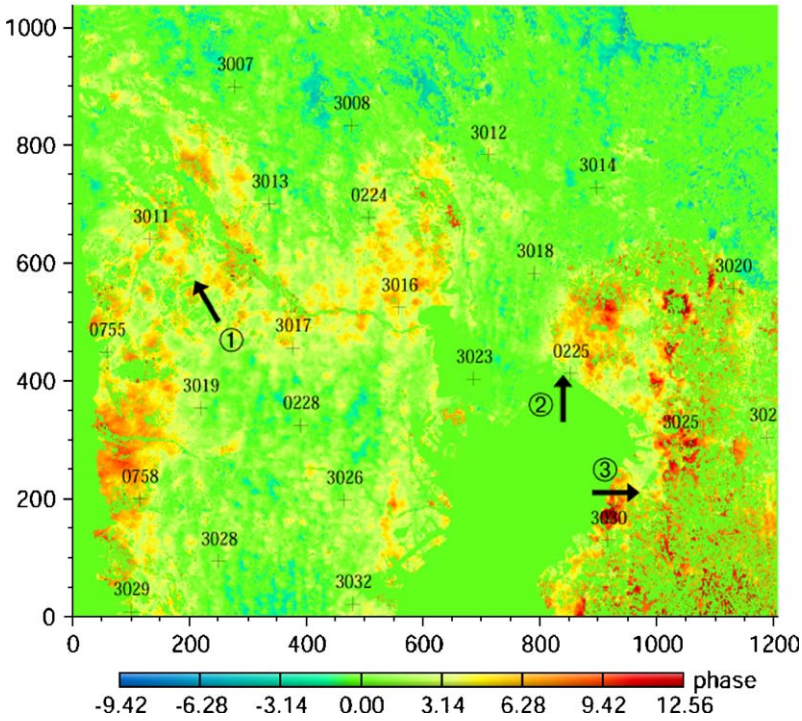

Fig. 8. Unwrapped phase after tropospheric delay mitigation.

regarded as reference pixel before and after the correction. The displacements of GPS stations, which are in good coherent regions, are projected into LOS direction and compared with InSAR range changes. The root of mean squares (RMS) decreased from 1.33 cm before correction to 0.87 cm after correction.

In area ①, more yellow patterns appear in the corrected image than that in the original one. Yonezawa and Takeuchi (2003) have shown that the maximum vertical displacement derived by InSAR and leveling measurement was about 3–4 cm in this area from the observation of 23 July 1995 to 15 March 1999. In our corrected image, it is about 1 cm from 8 February 1999 to 2 August 1999, which is consistent with Yonezawa and Takeuchi (2003). So the subsidence signal must have been partly counteracted by WSD. In area ②, no subsidence has been measured; however, there is about one fringe in the interferogram. After wet delay correction, part of the fringe has been removed. The displacements in LOS at S0225, for instance, are 2.53 and 0.61 cm before and after correction, respectively. The GPS displacement at this station is 0.76 cm. So the accuracy has been increased about 1.8 cm at S0225. The coherence is less than 0.2 in area ③, so we conclude that the red patterns are caused by the noise of decorrelation, instead of wet delay effect. Therefore, they cannot be removed by the correction of wet delay.

5. Conclusions and suggestions

Tropospheric delay effect is almost the most serious limitations for InSAR applications. From our WSD acquired by CGPS, the peak-to-peak value is up to 85.8 mm in the radar scene. Even after linear trend removal, the peak-to-peak value is still up to 40 mm. So we conclude that the deformation information is not reliable without mitigation of the tropospheric delay effect.

With GPS WZD parameters, the power semi-variogram model is fitted, and the parameters are 35.2, 3.6, and 0.88. In our opinion, the nugget effect has to be fitted, for which relate to measurement error and/or spatial sources of variation at distances smaller than the shortest sampling interval. Our estimation value of the power index, i.e. 0.88, is consistent with the former studies.

With GPS WZD parameters and the fitted semivariogram model, we predict the WSD for each pixel of the radar interferogram by UK algorithm. By comparison of unwrapped phase and CGPS range changes in LOS direction, the RMS decreased from 1.33 to 0.87 cm before and after correction. From our results, we can conclude that the GPS WZD parameters are effective to identify the geophysical signal, which do not appear in the interferogram, e.g. area ①, and mitigate the large-scale wet delay noise, e.g. area ②.

Different from GPS, in which the WZD is regarded as symmetrical in spatial and identical in several consecutive epochs, it has no redundant observations in InSAR because there is only one epoch and one zenith angle for each pixel. So we think that it is almost impossible to eliminate the tropospheric delay noise by InSAR itself under current conditions. Before the installation of InSAR constellation or multi-squint measurement, the calibration method may be an effective alternative. Since the sparse spatial resolution of GPS, the pixel-size resolution tropospheric delay parameters may be achieved by the integration of GPS, MERIS and other meteorology observations.

Acknowledgments

We are grateful to the two anonymous reviewers for their constructive comments. We thank Dr. Tim Wright and the reviewers for sharing their experience in using SNAPHU software. We acknowledge Dr. Jeffery T. Freymueller and Dr. Kristine M. Larson for the useful comments on GPS data processing with GIPSY-OASIS (II) software. We thank ESA and JAXA for providing ERS-2 SAR data, GSI of Japan for providing DEM and GPS data. GMS-5 images were provided by the weather homepage, Kochi University, for academic research and school education purpose. The GMT software was used to prepare figures (Wessel and Smith, 1998). This work was supported by a Specialized Research Fund for the Doctoral Program of Higher Education (No. 20030486038), a Program for New Century Excellent Talents in University (NCET-04-0681), the key laboratory of Geography Spatial Information, State Bureau of Surveying and Mapping (No. 1460130424210), the Open Research Fund Program of the Key Laboratory of Geomatics and Digital Technology, Shandong Province (No. SD040208), and the foundation of LOGEG State Bureau of Surveying and Mapping (No. 04-01-08).

References

Bean, B.R., Dutton, E.J., 1968. Radio Meteorology. Dover, New York.

Bevis, M., Chiswell, S., Businger, S., et al., 1996. Estimating wet delay using numerical weather analysis and predictions. Radio Science 31 (3), 477–487.

Bonforte, A., Ferretti, A., Prati, C., et al., 2001. Calibration of atmospheric effects on SAR interferograms by GPS and local atmosphere models: first results. Journal of Atmospheric and Solar-Terrestrial Physics 63, 1343–1357.

Buckley, S.M., Rosen, P.A., Hensley, S., et al., 2003. Land subsidence in Houston, Texas, measured by radar interferometry and constrained by extensometers. Journal of Geophysical Research 108 (B11), 2542.

Chen, C.W., 2001. Statistical-cost network-flow approaches to two-dimensional phase unwrapping for radar interferometry. Ph.D. Thesis, Stanford University.

Cressie, N., Hawkins, D.M., 1980. Robust estimation of the variogram: I. Mathematical Geology 12 (2), 115–125.

Delacourt, C., Briole, P., Achache, J., 1998. Tropospheric corrections of SAR interferograms with strong topography: application to Etna. Geophysical Research Letters 25 (15), 2849–2852.

Emardson, T.R., Simons, M., Webb, F.H., 2003. Neutral atmospheric delay in interferometric synthetic aperture radar applications: statistical description and mitigation. Journal of Geophysical Research 108 (B5), 2231–2238.

Goldstein, R., 1995. Atmospheric limitations to repeat-track radar interferometry. Geophysical Research Letters 22 (18), 2517–2520.

Goovaerts, P., 1997. Geostatistics for Natural Resources Evaluation. Oxford University Press, New York, Oxford.

Hanssen, R.F., 1998. Atmospheric Heterogeneities in ERS Tandem SAR Interferometry. Delft University Press, Delft, The Netherlands.

Hanssen, R.F., 2001. Rader Interferometry: Data Interpretation and Error Analysis. Kluwer Academic Publishers, Dordrecht.

Janssen, V., Ge, L., Rizos, C., 2004. Tropospheric corrections to SAR Interferometry from GPS observations. GPS Solutions 8 (3), 140–151.

Li, Z., Muller, J.-P., Cross, P., 2003. Tropospheric correction techniques in repeat-pass SAR interferometry. In: Proceeding of FRINGE 2003 Workshop, ESA ESRIN, Frascati, Italy, 1–5 December 2003.

Li, Z., Ding, X., Liu, G., 2004. Modelling atmospheric effects on InSAR with meteorological and continuous GPS observations: algorithms and some test results. Journal of Atmospheric and Solar-Terrestrial Physics 66, 907–917.

Li, Z., Muller, J.-P., Cross, P., et al., 2005. Interfermetric synthetic aperture radar InSAR atmospheric correction: GPS, Moderate Resolution Imaging Spectroradiometer (MODIS), and InSAR integration. Journal of Geophysical Research 110 (B03410).

Massonnet, D., Feigl, K.L., 1995. Discrimination of geophysical phenomena in satellite radar interferograms. Geophysical Research Letters 22 (12), 1537–1540.

Massonnet, D., Feigl, K.L., 1998. Radar interferometry and its application to changes in the Earth's surface. Reviews of Geophysics 36 (4), 441–500.

Massonnet, D., Feigl, K.L., Rossi, M., Adragna, F., 1994. Radar interferometric mapping of deformation in the year after the Landers earthquake. Nature 369, 227–230.

Rigo, A., Massonnet, D., 1999. Investigating the 1996 Pyrenean earthquake (France) with SAR interferograms heavily distorted by atmosphere. Geophysical Research Letters 26 (21), 3217–3220.

Rosen, P., Hensley, S., Joughin, I.R., et al., 2000. Synthetic aperture radar interferometry. Proceedings of IEEE 88 (3), 333–382.

Stein, A., Meer, F., Gorte, B., 2002. Spatial Statistics for Remote Sensing. Kluwer Academic Publishers, Dordrecht.

Tarayre, H., Massonnet, D., 1996. Atmospheric propagation heterogeneities revealed by ERS-1 interferometry. Geophysical Research Letters 23 (9), 989–992.

Treuhaft, R.N., Lanyi, G.E., 1987. The effect of the dynamic wet troposphere on radio interferometric measurements. Radio Science 22, 251–265.

Wadge, G., Webley, P.W., James, I.N., et al., 2002. Atmospheric models, GPS and InSAR measurements of the tropospheric water vapor field over Mount Etna. Geophysical Research Letters 29 (19), 11/1–11/4.

Webb, F.H., Zumberge, J.F., 1993. An Introduction to the GIPSY-OASIS(II). JPL Publ. D-11088, JPL, Pasadena, California.

Wessel, P., Smith, W.H.F., 1998. New, improved version of generic mapping tools released. EOS 79 (47), 579.

Williams, S., Bock, Y., Fang, P., 1998. Integrated satellite interferometry: tropospheric noise, GPS estimates and implications for interferometric synthetic aperture radar products. Journal of Geophysical Research 103 (B11), 27,051–27,067.

Yonezawa, C., Takeuchi, S., 2003. Effect of clouds on ERS SAR interferograms applied to land subsidence detection. International Journal of Remote Sensing 24 (1), 167–174.

Zebker, H.A., Rosen, P.A., Hensley, S., 1997. Atmospheric effect in interferometric synthetic aperture radar surface deformation and topographic maps. Journal of Geophysical Research 102 (B4), 7457–7563.